Thermoelectric properties of Ba 3 Co 2 O 6 (CO 3) 0.7 containing one-dimensional CoO 6 octahedral columns

Kouta Iwasaki, Teruhisa Yamamoto, Hisanori Yamane, Takashi Takeda, Shigeo Arai, Hidetoshi Miyazaki, Kazuyoshi Tatsumi, Masahito Yoshino, Tsuyoshi Ito, Yuji Arita, Shunsuke Muto, Takanori Nagasaki, and Tsuneo Matsui

Citation: Journal of Applied Physics **106**, 034905 (2009); doi: 10.1063/1.3174428
View online: http://dx.doi.org/10.1063/1.3174428
View Table of Contents: http://scitation.aip.org/content/aip/journal/jap/106/3?ver=pdfcov
Published by the AIP Publishing

Thermoelectric properties of $Ba_3Co_2O_6(CO_3)_{0.7}$ containing one-dimensional CoO_6 octahedral columns

Kouta Iwasaki,[1,a)] Teruhisa Yamamoto,[1] Hisanori Yamane,[2] Takashi Takeda,[3] Shigeo Arai,[4] Hidetoshi Miyazaki,[5] Kazuyoshi Tatsumi,[1] Masahito Yoshino,[1] Tsuyoshi Ito,[1] Yuji Arita,[4] Shunsuke Muto,[1] Takanori Nagasaki,[4] and Tsuneo Matsui[1,4]

[1]*Department of Materials, Physics and Energy Engineering, Graduate School of Engineering, Nagoya University, Furo-cho, Chikusa-ku, Nagoya 464-8603, Japan*

[2]*Institute of Multidisciplinary Research for Advanced Materials, Tohoku University, 2-1-1 Katahira, Aoba-ku, Sendai 980-8577, Japan*

[3]*National Institute for Materials Science (NIMS), 1-1 Namiki, Tsukuba 305-0044, Japan*

[4]*EcoTopia Science Institute, Nagoya University, Furo-cho, Chikusa-ku, Nagoya 464-8603, Japan*

[5]*UVSOR Facility, Institute for Molecular Science, Okazaki 444-8585, Japan*

(Received 17 April 2009; accepted 10 June 2009; published online 6 August 2009)

The thermoelectric properties of $Ba_3Co_2O_6(CO_3)_{0.7}$ have been investigated using prismatic single crystals elongated along the *c* axis. $Ba_3Co_2O_6(CO_3)_{0.7}$ has a pseudo-one-dimensional structure similar to that of 2H perovskite-type $BaCoO_3$ and contains CoO_6 octahedral columns running parallel to the *c* axis. The prismatic crystals are grown by a flux method using a $K_2CO_3-BaCl_2$ flux. The electrical conductivity (σ) along the columns (*c* axis) exhibits a metallic behavior (670–320 S cm^{-1} in the temperature range of 300–1100 K), whereas the temperature dependence of the electrical conductivity perpendicular to the *c* axis is semiconducting. The Seebeck coefficient (*S*) along the columns is positive and greater than 100 $\mu V\ K^{-1}$ over the measured temperature range (116–128 $\mu V\ K^{-1}$). $Ba_3Co_2O_6(CO_3)_{0.7}$ shows power factors (σS^2) of 5.5×10^{-4}–9.0×10^{-4} W m^{-1} K^{-2} above room temperature, relatively high values for an oxide material.
 [DOI: 10.1063/1.3174428]

I. INTRODUCTION

Thermoelectric power generation is a promising technique for an efficient use of energy since it can recycle waste heat into electricity. The energy conversion performance of thermoelectric materials is evaluated using the figure of merit (*Z*), defined as $Z=\sigma S^2/\kappa$ (where σ is the electrical conductivity, *S* is the Seebeck coefficient, and κ is the thermal conductivity). The numerator, σS^2, is related to electric power for thermoelectric power generation and is referred to as the power factor.

Among oxide ceramics, cobalt oxides have attracted attention as potential thermoelectric materials since the discovery of the large power factor of 5×10^{-3} W m^{-1} K^{-2} for Na_xCoO_2 crystals.[1] Na_xCoO_2 has a layered structure containing Co–O triangular lattices, in which edge-sharing CoO_6 octahedra are arranged two dimensionally. Both high electrical conductivity and high Seebeck coefficient have been observed along the Co–O triangular lattices in Na_xCoO_2. Considering that these electrical properties arise from the electronic structure formed by Co 3*d*-O 2*p* hybridization,[2,3] the relationship between thermoelectric properties and Co–O polyhedra is also of interest for other cobalt oxides.

Several cobalt oxides have pseudo-one-dimensional structures containing face-sharing CoO_6 polyhedral columns running parallel to the *c* axis.[4–16] For example, CoO_6 octahedra and CoO_6 triangular prisms alternately stack to form CoO_6 polyhedral columns in $Ca_3Co_2O_6$ [Fig. 1(a)].[4] $Sr_6Co_5O_{15-\delta}$ contains one-dimensional columns of four CoO_6 octahedra and one CoO_6 triangular prism [Fig. 1(b)],[5] and CoO_6 octahedral columns are formed in $BaCoO_3$ (2H perovskite-type structure) [Fig. 1(c)].[6] For $Ca_3Co_2O_6$ (Refs. 17–19) and $Sr_6Co_5O_{15-\delta}$,[20,21] *c*-axis elongated single crystals have been grown by flux methods, and the electrical properties along the CoO_6 polyhedral columns show a *p*-type semiconducting behavior. The power factors of $Ca_3Co_2O_6$ and $Sr_6Co_5O_{15-\delta}$ crystals are about one order of magnitude lower than that of the Na_xCoO_2 crystal because of their low elec-

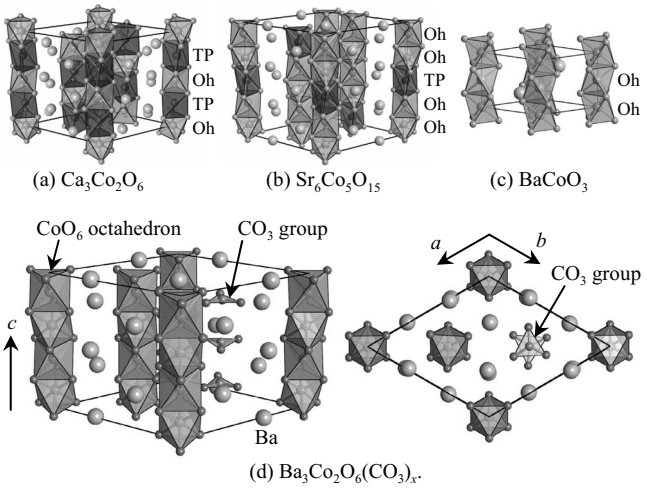

FIG. 1. Crystal structures of (a) $Ca_3Co_2O_6$, (b) $Sr_6Co_5O_{15}$, (c) $BaCoO_3$, and (d) $Ba_3Co_2O_6(CO_3)_x$. (Oh: CoO_6 octahedron; TP: CoO_6 triangular prism).

a)Author to whom correspondence should be addressed. Tel.: +81-52-789-4689. FAX: +81-52-789-3779. Electronic mail: k-iwasaki@nucl.nagoya-u.ac.jp.

trical conductivities ($\sigma \leq 100$ S cm^{-1}).[18–21] In these compounds with pseudo-one-dimensional structures, high electrical conductivity can be achieved by increasing the valence state of Co ions and/or reducing the CoO_6 prism content in the one-dimensional columns.[21] $Ba_3Co_2O_6(CO_3)_x$ contains CoO_6 octahedral columns with high valence state Co ions. As shown in Fig. 1(d), the crystal structure is similar to that of 2H perovskite-type $BaCoO_3$ [Fig. 1(c)],[6] but one-third of the CoO_6 octahedral columns are replaced by CO_3 groups, according to a powder neutron diffraction study reported by Boulahya *et al.*[7] for polycrystalline $Ba_3Co_2O_6(CO_3)_{0.6}$ [space group $P\bar{6}$, $a=9.683(1)$ Å, and $c=9.5180(8)$ Å]. The valence state of Co ions depends on the $[CO_3]^{2-}$ content and is generally regarded as $+(3+x)$. For example, the valence state of Co ions is +3.75 for a sample with no CO_3 defects ($x=0.75$). Since high electrical conductivity is expected for $Ba_3Co_2O_6(CO_3)_x$, its thermoelectric properties are of interest. In this paper, we report the preparation, electrical conductivity, and thermoelectric properties of the single crystal $Ba_3Co_2O_6(CO_3)_{0.7}$ ($Co^{+3.7}$). The anisotropic properties are also discussed.

II. EXPERIMENTAL

Single crystals of $Ba_3Co_2O_6(CO_3)_{0.7}$ were grown by a flux method. A mixture of K_2CO_3 (99.9%, Rare Metallic) and $BaCl_2$ (99%, Kojundo Chemical Laboratory) was used as a flux, and a mixture of Co_3O_4 (99.95%, Kanto Chemical) and $BaCO_3$ (99.99+%, Rare Metallic) powders was used as a solute. These reagents were weighed (12 g for K_2CO_3, 8 g for $BaCl_2$, 0.27 g for Co_3O_4, and 0.73 g for $BaCO_3$) and put into an Al_2O_3 crucible. The sample was heated at 1273 K for 2 h in air and cooled down to 873 K at a rate of 4 K/h followed by furnace cooling to room temperature. Then, the sample was washed with distilled water to remove the K_2CO_3–$BaCl_2$ flux.

X-ray diffraction (XRD) data were collected with a diffractometer (Rigaku, RINT2200) using Cu $K\alpha$ radiation with a pyrolytic graphite monochromator. Lattice parameters were refined by the Rietveld analysis using the program RIETAN-2000 (Ref. 22) with XRD data in the range of $10 \leq 2\theta \leq 80°$ (scan step of 0.03°) at room temperature. Electron diffraction images were observed with a transmission electron microscope (Hitachi, H-800) operated at an accelerating voltage of 200 kV. High resolution electron microscopic (HREM) images were taken at the Scherzer defocus using a 1000 kV microscope (the spherical aberration constant, $C_s=2.87$ mm) (Hitachi, H-1250ST). Simulated images were calculated by the multislice method using the MACTEMPAS software package. An infrared (IR) absorption spectrum was measured to confirm the existence of CO_3 groups (JASCO, FT/IR-610). The composition of the Ba:Co ratio was investigated by energy dispersive x-ray spectroscopic (EDS) analysis (JEOL, JSM-6460LA). Oxygen content was determined by an inert gas fusion–IR absorption method (HORIBA, EMGA-620W/C). Electrical conductivity (σ) was measured by the direct-current four-probe method in the temperature range from 300 to 1100 K in air. In the measurement, Pt wires were attached on a crystal using Au paste.

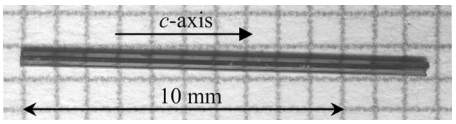

FIG. 2. Optical micrograph of a $Ba_3Co_2O_6(CO_3)_{0.7}$ single crystal.

Seebeck coefficient (S) was determined by the least-squares method from a plot of thermal electromotive force (ΔV) versus temperature difference (ΔT), and the contribution of Pt wires was subtracted. Thermal conductivity ($\kappa=b^2C_p^{-1}\rho^{-1}$) was calculated from thermal effusivity (b), specific heat (C_p), and bulk density (ρ). Thermal effusivity was measured by a laser thermoreflectance method (BETHEL, TM3), and specific heat was measured with a differential scanning calorimeter (NETZSCH, STA449C). Crystal structures were illustrated with the program VESTA.[23]

III. RESULTS AND DISCUSSION

A. Crystal growth

Black prismatic crystals elongated along the c axis were obtained by a flux method, as shown in Fig. 2. The maximum size of the obtained crystals was about $12 \times 0.5 \times 0.5$ mm^3. Figure 3 shows XRD patterns of (a) powdered crystals and (b) lateral planes of crystals. The XRD pattern of powdered crystals was consistent with a simulated pattern of the $Ba_3Co_2O_6(CO_3)_{0.6}$ structure [Fig. 3(a)],[7] and the lattice parameters were $a=9.6782(9)$ Å and $c=9.5156(9)$ Å. The XRD pattern of the lateral planes of crystals showed only $h00$ and $hk0$ peaks, as shown in Fig. 3(b), indicating that the prismatic crystals grew along the c axis.

A crystal structure analysis using an obtained crystal was unsuccessful since no $00l$ ($l=2n+1$, where n is an integer) peaks were observed by single crystal XRD. In contrast, as shown in Fig. 4, $00l$ ($l=2n+1$) peaks were confirmed by electron diffraction, as demonstrated by Boulahya *et al.*[7] Streaks perpendicular to the c^*-axis direction were also observed [Fig. 4(b)], which was similar to the case of polycrystalline $Ba_3Co_2O_6(CO_3)_{0.6}$.[7]

An IR spectrum of the obtained crystals showed an absorption peak at a 1450 cm^{-1} characteristic of carbonate groups, as shown in Fig. 5, indicating the existence of carbonate groups in the obtained crystals. EDS quantitative

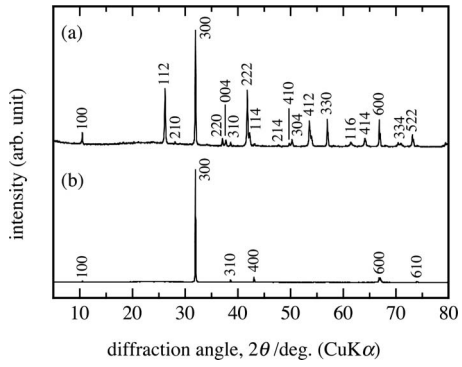

FIG. 3. (a) XRD patterns of powdered $Ba_3Co_2O_6(CO_3)_{0.7}$ crystals and (b) lateral planes of $Ba_3Co_2O_6(CO_3)_{0.7}$ crystals.

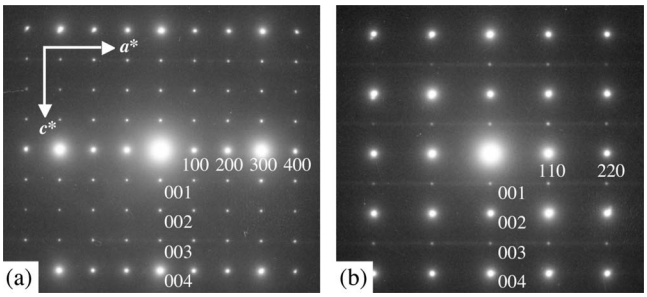

FIG. 4. Electron diffraction images of a $Ba_3Co_2O_6(CO_3)_{0.7}$ crystal along the following zone axes: (a) [010] and (b) [−110].

analysis confirmed a Ba/Co ratio of 1.48(6), consistent with the Ba/Co=1.5 expected from the chemical formula $Ba_3Co_2O_6(CO_3)_x$. No K, Cl, or Al contamination from the flux and crucible was detected in the obtained crystals. The oxygen content of the obtained crystals was 19.4(1) wt % according to inert gas fusion–IR absorption analysis. Consequently, the chemical composition of the obtained crystals was determined to be $Ba_3Co_2O_6(CO_3)_{0.7}$, assuming that the sample had no oxygen defects.

In the $Ba_3Co_2O_6(CO_3)_x$ structure, one may imagine that CO_3 groups could be irregularly replaced by CoO_6 octahedral columns, or vice versa. Figure 6 shows a HREM image of the *c* plane of a $Ba_3Co_2O_6(CO_3)_{0.7}$ crystal. The HREM image was consistent with the simulated image (crystal thickness, t=185 Å, and amount of defocus, Δf=550 Å) shown in the inset. Bright spots represent CO_3 groups, and the interval between the bright spots is 9.7 Å, comparable to the *a*-axis length of 9.6782(9) Å. Bright spots were regularly aligned over the entire field of view, but a few defects were also observed as indicated by white circles. These defects suggest irregular occupation by CoO_6 octahedral columns instead of CO_3 groups.

B. Thermoelectric properties

Figure 7 shows the Seebeck coefficient (S) of $Ba_3Co_2O_6(CO_3)_{0.7}$ along the *c* axis. S of $Ba_3Co_2O_6(CO_3)_{0.7}$ was positive and slightly increased with increasing temperature (116–128 μV K^{-1}). The positive sign of S indicates that holes are the dominant carrier in the measured temperature range, as is the case for $Ca_3Co_2O_6$ and $Sr_6Co_5O_{15}$, which have pseudo-one-dimensional structures.[18,19,21] The increase in S of $Ba_3Co_2O_6(CO_3)_{0.7}$ qualitatively corresponds to a metallic temperature dependence of electrical conductivity, as discussed below. S values of $Ba_3Co_2O_6(CO_3)_{0.7}$ are smaller than those of $Ca_3Co_2O_6$ (Ref. 18) and $Sr_6Co_5O_{15-\delta}$ (δ=0.7) (Ref. 21) at lower temperatures, and the S curves of the three compounds seem to converge with increasing temperature. In the direction perpendicular to the *c* axis, S of $Ba_3Co_2O_6(CO_3)_{0.7}$ was not accurately measured since the temperature difference between the two ends of an obtained crystal was slight due to its size of approximately 500 μm. The S value was about +30 μV K^{-1} at 300 K and increased with temperature (to about +100 μV K^{-1} at 600 K).

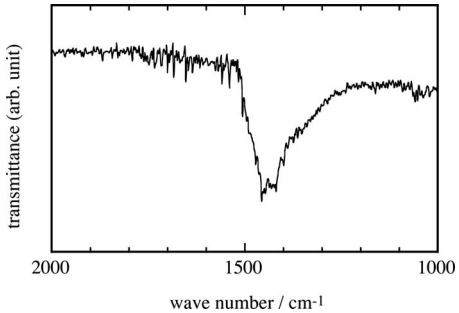

FIG. 5. IR spectrum of $Ba_3Co_2O_6(CO_3)_{0.7}$ crystals.

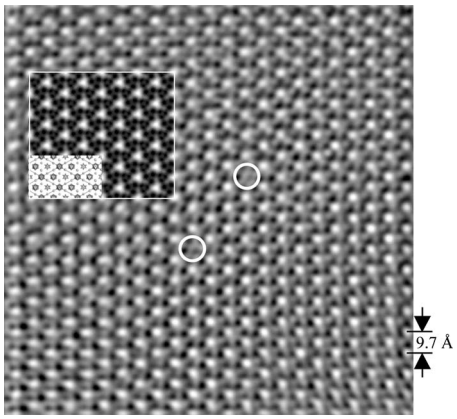

FIG. 6. HREM image of a $Ba_3Co_2O_6(CO_3)_{0.7}$ crystal along [001]. A calculated HREM image and the *c* plane of $Ba_3Co_2O_6(CO_3)_{0.7}$ are also included. White circles indicate defects of bright spots.

Figure 8 shows the electrical conductivity (σ) of $Ba_3Co_2O_6(CO_3)_{0.7}$ along and perpendicular to the *c* axis. σ along the *c* axis exhibited a metallic behavior, as shown in the upper figure (670–320 S cm^{-1} in the temperature range of 300–1100 K), whereas other cobalt oxides containing CoO_6 polyhedral one-dimensional columns exhibited a semiconducting behavior,[17–21,24–28] e.g., $Ca_3Co_2O_6$ (Refs. 17–19) and $Sr_6Co_5O_{15-\delta}$ (Refs. 20 and 21) crystals. For Na_xCoO_2 containing two-dimensional Co–O triangular lattices, the metallic temperature dependence of electrical conductivity with a high positive Seebeck coefficient arises from its electronic structure in which the Fermi level is located just below the upper end of the valence band formed by Co 3*d*-O 2*p* hybridization.[3] A similar electronic structure may well be formed along the one-dimensional CoO_6 octahedral columns for $Ba_3Co_2O_6(CO_3)_{0.7}$. Considering that σ of

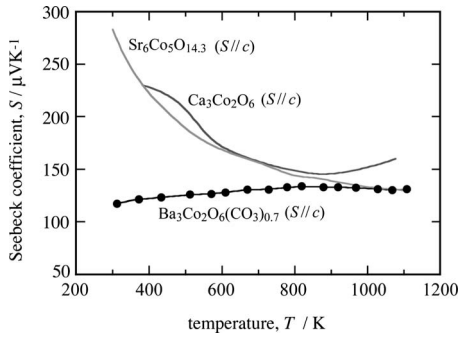

FIG. 7. Temperature dependence of the Seebeck coefficients of $Ba_3Co_2O_6(CO_3)_{0.7}$, $Ca_3Co_2O_6$ (Ref. 18), and $Sr_6Co_5O_{15-\delta}$ (δ=0.7) (Ref. 21) along the *c* axes.

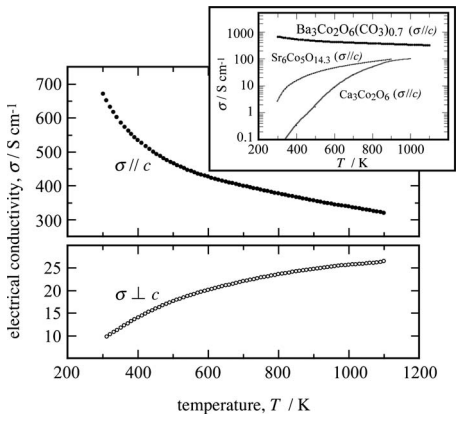

FIG. 8. Temperature dependence of the electrical conductivity of $Ba_3Co_2O_6(CO_3)_{0.7}$ along and perpendicular to the c axis. The inset shows the electrical conductivities of $Ba_3Co_2O_6(CO_3)_{0.7}$, $Ca_3Co_2O_6$ (Ref. 18), and $Sr_6Co_5O_{15-\delta}$ (δ=0.7) (Ref. 21) along the c axes.

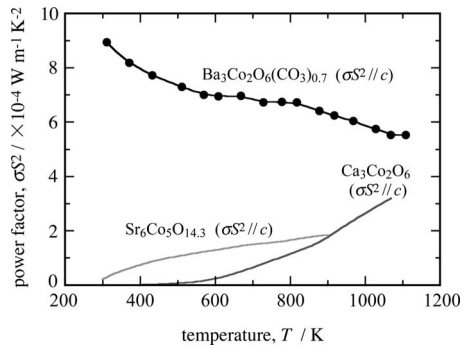

FIG. 9. Temperature dependence of the power factors of $Ba_3Co_2O_6(CO_3)_{0.7}$, $Ca_3Co_2O_6$ (Ref. 18), and $Sr_6Co_5O_{15-\delta}$ (δ=0.7) (Ref. 21) along the c axes.

$Ba_3Co_2O_6(CO_3)_{0.7}$ is higher than those of $Ca_3Co_2O_6$ and $Sr_6Co_5O_{15-\delta}$, as shown in the inset, a high carrier concentration would result from a high valence state of Co ions ($Co^{+3.7}$) in $Ba_3Co_2O_6(CO_3)_{0.7}$. Alternatively, high carrier mobility may arise from an absence of CoO_6 triangular prisms that cause a narrow band width because of its Co–O distances longer than those in CoO_6 octahedra.

At the beginning of the electrical conductivity measurement, σ along the c axis at 300 K was 830 S cm^{-1}, but it decreased to 670 S cm^{-1} during repeated measurements in the temperature range of $300 \leq T \leq 1100$ K in air. Since the $Ba_3Co_2O_6(CO_3)_x$ phase is stable below 1100 K in air, the decrease in σ is attributable to a decrease in carrier (hole) concentration caused by a reduction in CO_3 content and a decrease in carrier mobility caused by the distortion of crystallinity due to a release of CO_3 groups. The fraction of CO_3 released during the measurements was estimated to be 0.02 $[Ba_3Co_2O_6(CO_3)_{0.68}]$ by thermogravimetric analysis.

In the direction perpendicular to the c axis, σ exhibited a semiconducting behavior, in contrast to the metallic behavior along the c axis, as shown in the bottom figure. Moreover, the values were more than one order of magnitude smaller than those along the c axis. This anisotropy in σ indicates that the CoO_6 octahedral columns are conductive, and carrier conduction between the columns is scattered by insulating Ba–O phases and CO_3 groups.

As shown in Fig. 9, the power factor (σS^2) of $Ba_3Co_2O_6(CO_3)_{0.7}$ along the c axis decreased with increasing temperature mainly because of the decrease in electrical conductivity (Fig. 7). The σS^2 values were larger than those of $Ca_3Co_2O_6$ (Ref. 18) and $Sr_6Co_5O_{15-\delta}$ (δ=0.7) (Ref. 21) crystals along the CoO_6 polyhedral columns. The value of 9.0×10^{-4} W m^{-1} K^{-2} at 300 K is relatively high for an oxide ceramic and is comparable to the value of 1×10^{-3} W m^{-1} K^{-2} used as a standard to evaluate potential as a thermoelectric material.

Table I summarizes the thermal conductivity (κ), power factor, and figure of merit ($Z=\sigma S^2 \kappa^{-1}$) of $Ba_3Co_2O_6(CO_3)_{0.7}$ at 300 K together with those of a $Na_xCoO_{2-\delta}$ crystal along the Co–O triangular lattices.[29] κ of $Ba_3Co_2O_6(CO_3)_{0.7}$ along the c axis was 17.7 W m^{-1} K^{-1}, about 15 times larger than that perpendicular to the c axis (1.20 W m^{-1} K^{-2}). This anisotropy in κ indicates that heat mainly conducts through the CoO_6 octahedral columns, and phonon is significantly scattered by Ba atoms and CO_3 groups between the columns. Since the thermal conductivity of charged carriers (κ_c) along the c axis is calculated to be 0.49 W m^{-1} K^{-1} at 300 K from the Wiedemann–Franz law ($\kappa_c=\sigma LT$, where L is the Lorenz number$=2.45 \times 10^{-8}$ V^2 K^{-2}), the contribution of thermal conduction by phonon to κ is dominant. The figure of merit of $Ba_3Co_2O_6(CO_3)_{0.7}$ along the c axis was $Z=5.1 \times 10^{-5}$ K^{-1} at 300 K, smaller than that of $Na_xCoO_{2-\delta}$ mainly because of the difference in power factor, which was caused by the higher electrical conductivity of $Na_xCoO_{2-\delta}$ (σ =3450 S cm^{-1} at 300 K).[29]

IV. CONCLUSION

Prismatic single crystals elongated along the c axis of $Ba_3Co_2O_6(CO_3)_{0.7}$ were grown by a flux method. The temperature dependence of the electrical conductivity along the CoO_6 octahedral columns (c axis) was metallic above 300 K, whereas other cobalt oxides containing one-dimensional CoO_6 polyhedral columns behaved as insulators. Since the high electrical conductivity of $Ba_3Co_2O_6(CO_3)_{0.7}$ is due to the CoO_6 octahedral columns, similar electrical properties would be expected for 2H perovskite-type $BaCoO_3$ along the c axis, although the electrical conductivity of its polycrystalline sample is relatively low.[24,25] The power factors of 5.5×10^{-4}–9.0×10^{-4} W m^{-1} K^{-2} above 300 K for $Ba_3Co_2O_6(CO_3)_{0.7}$ were larger than any other reported value for cobalt oxides having pseudo-one-dimensional structures. Since its power factor is relatively high for an oxide material, further studies on the thermoelectric properties of $Ba_3Co_2O_6(CO_3)_x$ are necessary. The optimization of carrier

TABLE I. Thermal conductivity (κ), power factor (σS^2), and figure of merit ($Z=\sigma S^2 \kappa^{-1}$) of $Ba_3Co_2O_6(CO_3)_{0.7}$ at 300 K.

	κ (W m^{-1} K^{-1})	σS^2 (W m^{-1} K^{-2})	Z (K^{-1})
$Ba_3Co_2O_6(CO_3)_{0.7}$ (//c)	17.7	9.0×10^{-4}	5.1×10^{-5}
$Ba_3Co_2O_6(CO_3)_{0.7}$ ($\perp c$)	1.20	8.8×10^{-7}	7.3×10^{-7}
$Na_xCoO_{2-\delta}$ ($\perp c$) (Ref. 29)	19.0	23.8×10^{-4}	12.5×10^{-5}

concentration and the reduction in thermal conductivity is currently underway in order to maximize the thermoelectric properties.

ACKNOWLEDGMENT

This study was partly supported by Grant-in-Aid 20760465 from the Ministry of Education, Culture, Sports, Science and Technology of Japan (MEXT).

[1]I. Terasaki, Y. Sasago, and K. Uchinokura, Phys. Rev. B **56**, R12685 (1997).
[2]D. J. Singh, Phys. Rev. B **61**, 13397 (2000).
[3]T. Takeuchi, T. Kondo, T. Takami, H. Takahashi, H. Ikuta, U. Mizutani, K. Soda, R. Funahashi, M. Shikano, M. Mikami, S. Tsuda, T. Yokoya, S. Shin, and T. Muro, Phys. Rev. B **69**, 125410 (2004).
[4]H. Fjellvåg, E. Gulbrandsen, S. Aasland, A. Olsen, and B. C. Hauback, J. Solid State Chem. **124**, 190 (1996).
[5]W. T. A. Harrison, S. L. Hegwood, and A. J. Jacobson, J. Chem. Soc., Chem. Commun. **1953** (1995).
[6]H. Taguchi, Y. Takeda, F. Kanamaru, M. Shimada, and M. Koizumi, Acta Crystallogr., Sect. B: Struct. Crystallogr. Cryst. Chem. **33**, 1298 (1977).
[7]K. Boulahya, U. Amador, M. Parras, and J. M. González-Calbet, Chem. Mater. **12**, 966 (2000).
[8]O. Gourdon, V. Petricek, M. Dusek, P. Bezdicka, S. Durovic, D. Gyepesova, and M. Evain, Acta Crystallogr., Sect. B: Struct. Sci. **55**, 841 (1999).
[9]J. M. Perez-Mato, M. Zakhour-Nakhl, F. Weill, and J. Darriet, J. Mater. Chem. **9**, 2795 (1999).
[10]K. Boulahya, M. Parras, and J. M. González-Calbet, J. Solid State Chem. **142**, 419 (1999).
[11]K. Boulahya, M. Parras, and J. M. González-Calbet, J. Solid State Chem. **145**, 116 (1999).
[12]K. Boulahya, M. Parras, J. M. González-Calbet, and A. Vegas, J. Solid State Chem. **151**, 77 (2000).
[13]K. Boulahya, M. Parras, and J. M. González-Calbet, Chem. Mater. **12**, 25 (2000).
[14]K. Boulahya, M. Parras, and J. M. González-Calbet, Chem. Mater. **12**, 2727 (2000).
[15]A. El Abed, S. E. Elqebbaj, M. Zakhour, M. Champeaux, J. M. Perez-Mato, and J. Darriet, J. Solid State Chem. **161**, 300 (2001).
[16]J. M. González-Calbet, K. Boulahya, M. L. Ruiz, and M. Parras, J. Solid State Chem. **162**, 322 (2001).
[17]A. Maignan, C. Michel, A. C. Masset, C. Martin, and B. Raveau, Eur. Phys. J. B **15**, 657 (2000).
[18]M. Mikami, R. Funahashi, M. Yoshimura, Y. Mori, and T. Sasaki, J. Appl. Phys. **94**, 6579 (2003).
[19]J. Takahashi, H. Yamane, and M. Shimada, Jpn. J. Appl. Phys., Part 2 **43**, L331 (2004).
[20]J. Sun, G. Li, Z. Li, L. You, and J. Lin, Inorg. Chem. **45**, 8394 (2006).
[21]K. Iwasaki, T. Murase, T. Ito, M. Yoshino, T. Matsui, T. Nagasaki, and Y. Arita, Jpn. J. Appl. Phys., Part 1 **46**, 256 (2007).
[22]F. Izumi and T. Ikeda, Mater. Sci. Forum **321–324**, 198 (2000).
[23]K. Momma and F. Izumi, J. Appl. Crystallogr. **41**, 653 (2008).
[24]K. Yamaura, H. W. Zandbergen, K. Abe, and R. J. Cava, J. Solid State Chem. **146**, 96 (1999).
[25]K. Yamaura and R. J. Cava, Solid State Commun. **115**, 301 (2000).
[26]K. Iwasaki, H. Yamane, S. Kubota, J. Takahashi, and M. Shimada, J. Alloys Compd. **358**, 210 (2003).
[27]K. Iwasaki, M. Shimada, H. Yamane, J. Takahashi, S. Kubota, T. Nagasaki, Y. Arita, J. Yuhara, Y. Nishi, and T. Matsui, J. Alloys Compd. **377**, 272 (2004).
[28]T. Takami, H. Ikuta, and U. Mizutani, Jpn. J. Appl. Phys., Part 1 **43**, 8208 (2004).
[29]K. Fujita, T. Mochida, and K. Nakamura, Jpn. J. Appl. Phys., Part 1 **40**, 4644 (2001).